Article

Experimental Study of Airfoil Leading Edge Combs for Turbulence Interaction Noise Reduction

Thomas Fritz Geyer [1],*, Sahan Hasaranga Wasala [2] and Ennes Sarradj [3]

[1] Technical Acoustics Group, Brandenburg University of Technology Cottbus—Senftenberg, 03046 Cottbus, Germany

[2] Department of Engineering Science, University of Auckland, Auckland 1142, New Zealand; swas118@aucklanduni.ac.nz

[3] Institute of Fluid Mechanics and Engineering Acoustics, Technical University Berlin, 10587 Berlin, Germany; ennes.sarradj@tu-berlin.de

* Correspondence: thomas.geyer@b-tu.de; Tel.: +49-355-69-5012

check for updates

Abstract: The interaction of a turbulent flow with the leading edge of a blade is a main noise source mechanism for fans and wind turbines. Motivated by the silent flight of owls, the present paper describes an experimental study performed to explore the noise-reducing effect of comb-like extensions, which are fixed to the leading edge of a low-speed airfoil. The measurements took place in an aeroacoustic wind tunnel using the microphone array technique, while the aerodynamic performance of the modified airfoils was captured simultaneously. It was found that the comb structures lead to a noise reduction at low frequencies, while the noise at high frequencies slightly increases. The most likely reasons for this frequency shift are that the teeth of the combs break up large incoming turbulent eddies into smaller ones or that they shift turbulent eddies away from the airfoil surface, thereby reducing pressure fluctuations acting on the airfoil. The aerodynamic performance does not change significantly.

Keywords: wind turbine; leading edge noise; turbulence interaction noise; comb

1. Introduction

When turbulent eddies interact with the blade of a fan or a wind turbine, noise is generated at the leading edge. In the case of an industrial fan, this happens for example when the fan is mounted downstream of a heat exchanger. For wind turbines, the planetary boundary layer contains intense atmospheric turbulence with a wide range of length scales. The interaction of the blades with this turbulence is considered to be a significant noise generation mechanism, especially when the leading edge radius is small (i.e., the blade is sharp) compared to the length scale of the turbulent eddies. Experimental studies on the reduction of turbulence interaction noise mainly focus on modifying the blade geometry. This can be done by using serrated edges, as for example examined by Soderman [1], Hersh et al. [2], Gruber et al. [3], Roger et al. [4], Liu et al. [5], Narayanan et al. [6] and Juknevicius and Chong [7]. A similar approach is the use of so-called wavy (or sinusoidal) leading edges, which has been investigated by Hansen et al. [8], Polacsek et al. [9], Clair et al. [10], Chong et al. [11], Chaitanya et al. [12,13] and Biedermann et al. [14,15], among others. More recently, the use of airfoils with slitted leading edges has been investigated [16]. Another possible method is the modification of the material of the leading edge, for example by using flow-permeable materials [4,17,18]. Besides the experimental work, there are also some analytical and numerical investigations. These include serrated and wavy leading edges [19–27] as well as porous materials [28,29]. Another recent numerical study was performed on the potential noise reduction of a blade with a leading-edge modified with hooks [30]. These hooks were inspired by the extensions that can be found on the first primary feather of owl wings [31,32].

Past studies of the silent flight of owls suggest that these leading-edge hooks rather serve an aerodynamic purpose by controlling separation [33,34]. A recent investigation [32] supports these findings by showing that at moderate angles of attack the influence of the hooks on the noise reduction is negligible, while at large angles a small noise reduction was observed. Nevertheless, the potential noise reduction through using structures similar to a comb still seems worth examining. The present paper describes an experimental study of the noise generated by airfoils whose leading edges are modified using comb-like extensions, focusing on the noise generated by the interaction of the airfoil leading edge with turbulence in the incoming flow (turbulence interaction noise). Thereby, the aim was to test different leading-edge combs with varying geometrical parameters and to identify the ones that will result in a reduction of turbulence interaction noise without giving a large aerodynamic penalty.

The remainder of this paper is organized as follows: first, the experimental setup will be explained, including the aeroacoustic wind tunnel and the grids used for the generation of the incident turbulence, the airfoils modified with leading-edge comb structures, the wind tunnel balance used for the measurement of the aerodynamic forces acting on the airfoils and the microphone array measurement technique. Then, the results of the acoustic and aerodynamic measurements will be presented and discussed. Finally, the findings of the study will be summarized.

2. Experimental Setup

2.1. Wind Tunnel

All measurements took place in the small aeroacoustic open jet wind tunnel at the Brandenburg University of Technology, using a circular nozzle with an exit diameter of 0.2 m [35]. The maximum flow speed with this nozzle is approximately 92 m/s. The wind tunnel provides a very quiet flow that allows for a high signal-to-noise ratio, while at the same time the turbulence intensity in the core jet is well below 1%. A photograph of the setup is shown in Figure 1a, a corresponding schematic in Figure 1b. During acoustic measurements, the test section is surrounded by a chamber that has absorbing walls on three sides with a microphone array for a ceiling (see Figure 1a). The dimensions of the chamber are 2.0 m (length) × 1.55 m (width) × 1.5 m (height). The absorbing sidewalls lead to a quasi-anechoic environment inside the tunnel for frequencies above approximately 125 Hz.

(a)
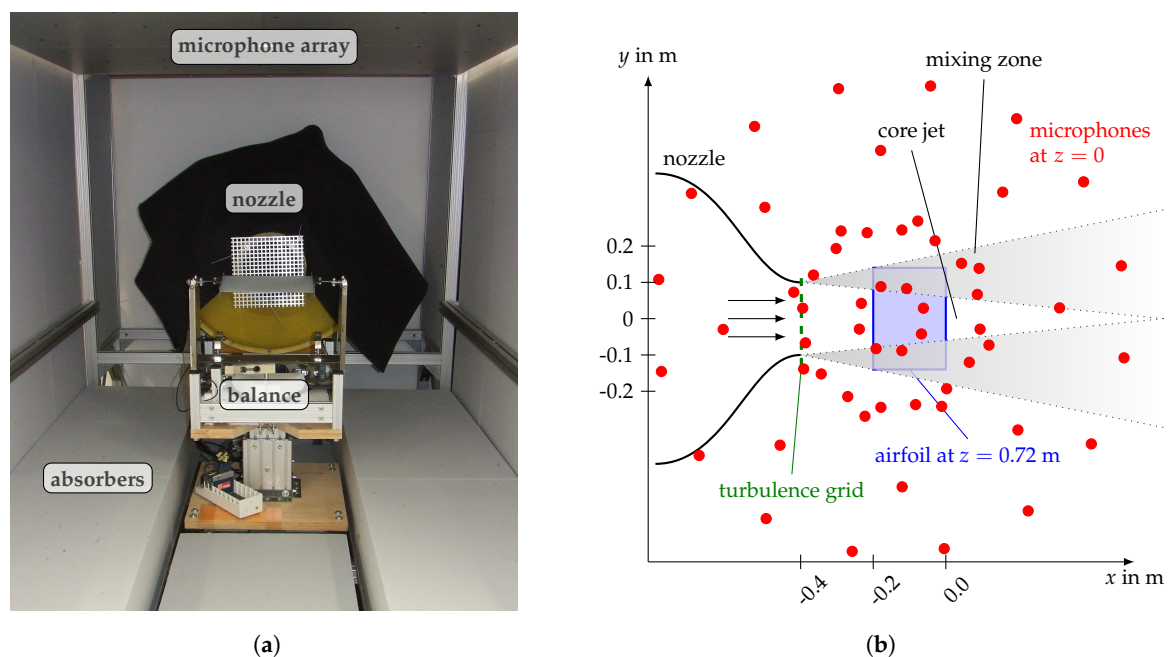

(b)

Figure 1. (**a**) Photograph (taken from downstream direction) and (**b**) schematic (top view) of the measurement setup inside the aeroacoustic wind tunnel facility.

2.2. Generation of Incident Turbulence

The incident turbulence required for the generation of leading-edge noise was produced using turbulence grids mounted to the nozzle of the wind tunnel. In order to be able to vary the turbulent inflow conditions, two perforated plates with square holes (PPS) of different geometry were used. Their parameters are summarized in Table 1. The different porosities of the two grids, defined as the ratio of the open surface to the total surface, lead to different pressure losses over the grids. In turn, this results in different maximum flow speeds due to the fact that there is an upper limit for the total pressure that can be provided by the 18.5 kW fan of the aeroacoustic wind tunnel.

Table 1. Overview of turbulence grids used in the experiments (PPS; perforated plate with square holes).

Grid no.	Description	Mesh Width W (mm)	Bar Width b (mm)	Porosity σ (%)
1	PPS 12/2	12	2	69
2	PPS 14/4	14	4	51

It is known that grid-generated turbulence decays rapidly and is quasi-isotropic and homogeneous at distances greater than approximately 10 mesh widths downstream of the grid [36–38]. For the grids used in the present setup, this would correspond to a minimum distance of 0.14 m. In the end, a greater distance of 0.2 m between the turbulence grid and the leading edge of the airfoils was chosen. In order to determine the turbulence parameters at this distance, Constant Temperature Anemometry (CTA) measurements were performed using a Dantec 55P11-type single wire probe and a Dantec multi-channel CTA measurement system. The probe was positioned using a 3D traverse system made by Isel, which has a minimum step size of 0.1 mm. Measurements were conducted at 30 positions randomly distributed on a plane normal to the flow, which had a size of 56 mm × 56 mm (corresponding to 4 mesh widths × 4 mesh widths of the PPS 14/4 turbulence grid). The data were recorded with a sampling frequency of 25.6 kHz over a measurement duration of 12 s. To avoid the possible influence of vibrations of the traverse system after each step, the first 2 s from each time series were omitted, leaving 256,000 samples to be analyzed. As described in [38], the turbulence length scale Λ_x was determined by fitting the one-sided power spectrum of the measured velocity fluctuations to

$$G_{uu}(f) = \frac{4\tilde{u}^2\Lambda_x}{U\left(1 + \left(\frac{2\pi f \Lambda_x}{U}\right)^2\right)}, \tag{1}$$

which is a formulation for isotropic and homogeneous turbulence given in [39]. In Equation (1), f is the frequency, U is the mean value and $\tilde{u}$ is the RMS value of the velocity fluctuations. The resulting turbulence intensities for both grids are shown in Figure 2a for a distance of 0.2 m from the grid, which corresponds to the location of the airfoil leading edge in the acoustic measurements. The corresponding turbulence length scales are then shown in Figure 2b.

The PPS 12/2 grid produces turbulence with an intensity that increases from 2.6% at low flow speeds up to 6.2% at the highest flow speed of 73.3 m/s at this distance. The integral length scale takes values between 4.9 mm and 5.6 mm. The turbulence intensity produced by the PPS 14/4 grid does not vary as much with the flow speed. It takes values between 4.7% and 5.1%, while the integral length scale is between 5.3 mm and 6.0 mm. For both grids, the standard deviation of turbulence intensity and integral length scale are very small, confirming that the turbulence at a distance of 0.2 m from the grid is homogeneous. The turbulence intensity without a grid mounted to the nozzle is below 1%.
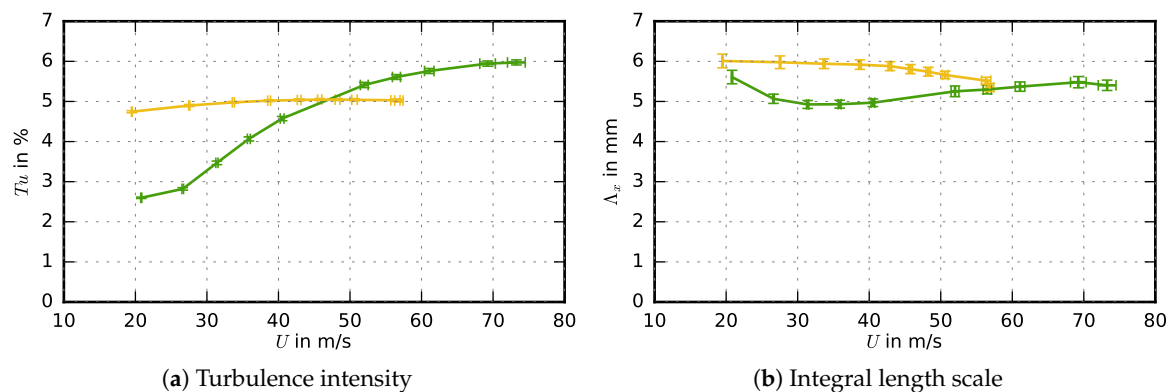
(a) Turbulence intensity   **(b)** Integral length scale

Figure 2. (**a**) Intensity and (**b**) integral length scale of the turbulence generated by the two perforated plates given in Table 1, measured at 30 points in a plane normal to the flow, at the position of the leading edge (given are the mean values as well as the standard deviations), ▬ PPS 12/2, ▬ ▬ PPS 14/4.

2.3. Leading Edge Comb Structures

To examine the possible reduction of turbulence interaction noise through leading-edge comb structures, different types of combs were mounted to the leading edge of a NASA/Langley LS(1)-0413 airfoil. This airfoil is a 13% thick low-speed airfoil used in small wind turbines, such as the CART-2 and CART-3. It has a chord length c_l of 0.2 m and a span width b of 0.28 m. The airfoil was made using Selective Laser Sintering (SLS). It consists of a main body, shown in Figure 3a, in which different leading edges can be inserted. Several methods were tried to build the desired leading-edge combs, such as 3D-printing. In the end, the combs were made from thin steel pins that have a diameter of 0.7 mm, which were inserted into a leading-edge insert that contained regular holes of ≤0.8 mm diameter (see Figure 3b). The combs are characterized by three parameters: their length h, their spacing s, and their shape, which could either be straight or slightly upward curved with an angle β of approximately 15°. A corresponding schematic is shown in Figure 4. In the end, eleven different combinations were tested. Table 2 gives an overview of the comb structures examined in the present study. Thereby, the pins were not distributed along the complete span of the airfoil, but only over the center part that had a spanwise width of 0.2 m (which corresponds to the exit diameter of the nozzle). Figure 5 shows a photograph of the airfoil with a comb with curved teeth of 12 mm and 20 mm length (no. 11 in Table 2).

Table 2. Overview of comb structures used in the experiments (see schematic in Figure 4 for details).

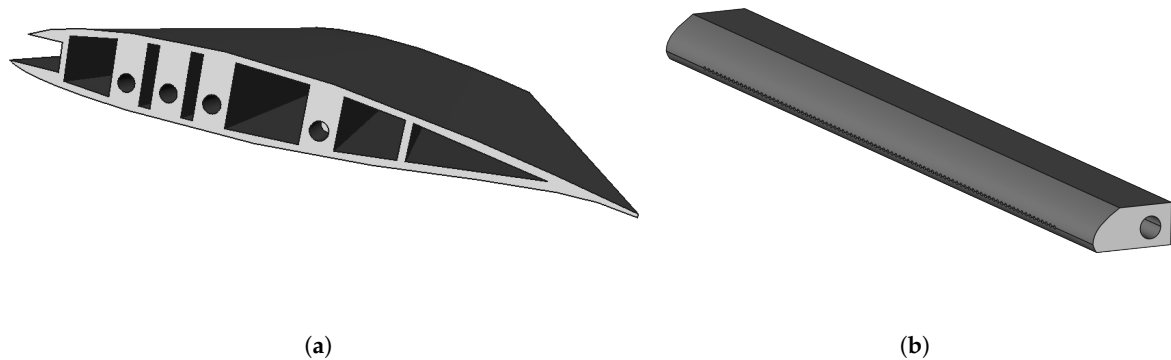| No.	Normalized Teeth Length h/c_l	Normalized Spacing between Teeth s/c_l	Shape
1	0.1	0.038	straight
2	0.06	0.038	straight
3	0.1	0.019	straight
4	0.06	0.019	straight
5	0.06/0.1 (alternating)	0.019	straight
6	0.1	0.0095	straight
7	0.06	0.0095	straight
8	0.1	0.038	curved
9	0.06	0.038	curved
10	0.06	0.019	curved
11	0.06/0.1 (alternating)	0.019	curved

Figure 3. Computer-aided design (CAD) model of the airfoil, (**a**) main body without leading edge inserted and (**b**) leading edge insert without pins.
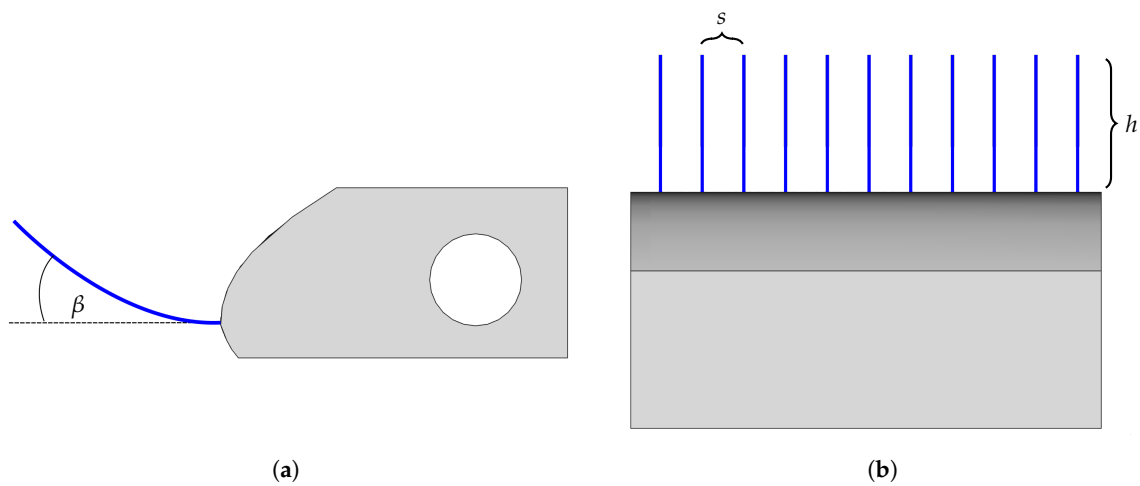

Figure 4. Schematic of the comb structures used in the present study, gray: leading edge insert, blue: teeth of the comb, (**a**) side view, (**b**) top view, detail.
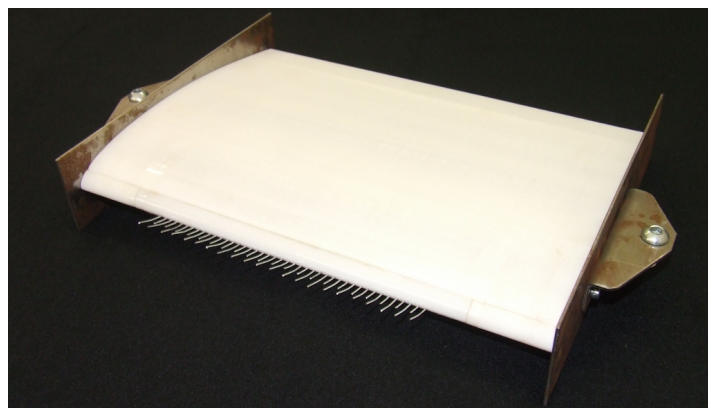

Figure 5. Photograph of the airfoil used for the present investigation (with curved teeth of 12 mm and 20 mm length).

An unmodified LS(1)-0413 airfoil served as a baseline. No tripping device was used for the experiments.

2.4. Aerodynamic Measurements

The aerodynamic performance of the airfoils was captured using a six-component balance (visible in Figure 1a). The airfoil was attached to the balance at the sides and both tips were outside the flow. The data from the six single point load cells, which have a nominal load of 10 kg, were recorded with a sampling frequency of 1 kHz and a measurement duration of 10 s using two National Instruments 24-bit full-bridge analog input modules. From these data, the time-averaged lift and drag forces were calculated. Due to the fact that the present aerodynamic measurements were performed in an open jet setup, which consists of a conical core jet with expanding shear layers, the results cannot be directly compared to values obtained in a closed test section. Thus, the measured lift and drag forces only serve as a means to compare the aerodynamic performance of the modified airfoils to that obtained for the baseline airfoil in the same setup.

The presence of an airfoil inside an open jet induces a deflection of the jet and a curvature of the shear layer, leading to the fact that the geometric angle of attack that is adjusted in such a setup differs from the so-called effective angle of attack that would be obtained in free-flow conditions. Unfortunately, existing correction methods like that proposed by Brooks et al. [40] are not applicable in the present case of cambered airfoils in an open jet. Hence, the geometric angles of attack given here have to be understood as a description of different configurations only.

In total, measurements were performed at geometric angles of attack of 0°, 6° and 12° for both turbulence grids from Table 1. For each configuration, measurements were made at ten flow speeds, corresponding to those shown in Figure 2a. The maximum flow speed is 73 m/s (chord-based Reynolds number $Re = 965{,}000$, Mach number $M = 0.21$) for the PPS 12/2 grid and 56 m/s ($Re = 740{,}000$, $M = 0.16$) for the PPS 14/4 grid. For brevity, however, only selected results will be presented.

2.5. Microphone Array and Data Processing

All acoustic measurements were conducted using a planar 56-channel microphone array, which was positioned out of the flow at a distance of 0.72 m above the airfoil (see Figure 1). To account for the error in source localization due to the refraction of sound at the wind tunnel shear layer, a correction method based on ray tracing was applied [41]. Thereby, a thick shear layer around a conical jet was assumed.

For each microphone array measurement, 40 s of data were recorded with a sampling frequency of 51.2 kHz, using a National Instruments 24-bit multichannel measurement system. In post-processing the recorded time-data were first Fourier-transformed into the frequency domain. This was done block-wise with blocks of 4096 samples length, using a Hanning window and an overlap of 50%. This lead to a total of 1000 blocks. Then, the cross spectral matrices were further processed by removing the main diagonal and applying the CLEAN-SC algorithm developed by Sijtsma [42]. The algorithm was used on a fully three-dimensional source region with dimensions of 0.6 m (chordwise direction) × 0.6 m (spanwise direction) × 0.4 m (vertical direction). With an increment of 0.01 m this lead to a total of 152,561 grid points. The chosen steering vector for the beamforming was that corresponding to Formulation IV in [43]. The outcome from this beamforming are three-dimensional maps of acoustic source positions, so-called 3D sound maps. A sample sound map is shown in Figure 6. In this map, the anticipated noise sources are already visible: the main source at the leading edge of the airfoil, another strong source at the turbulence grid and two weaker sources at the position where the wind tunnel shear layer interacts with the airfoil trailing edge.

In order to obtain sound pressure level spectra for the noise generated at the leading edge of the airfoil due to the interaction with the turbulence produced by the turbulence grids, all noise sources in the sound map that are positioned within a certain three-dimensional volume were integrated. In the present case, the chosen leading-edge integration volume has an extent of 0.12 m in all three directions in space and contained only the center part of the leading edge. Unwanted background noise sources, such as the turbulence grid, the airfoil trailing edge or the side regions where the wind tunnel shear layer interacts with the airfoil, were excluded from the integration. The chosen integration volume

is depicted in Figure 6. Finally, the integrated sound pressures were converted to third-octave band sound pressure levels L_p.
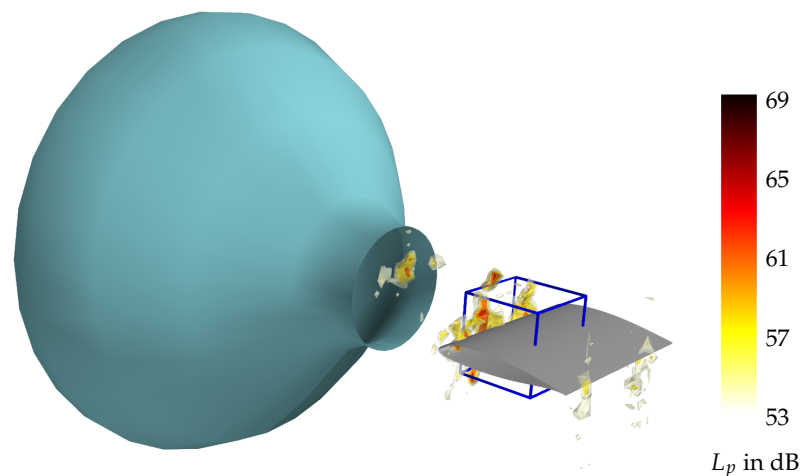

Figure 6. Sample sound map of the noise from the reference airfoil at a Mach number M = 0.21, geometric angle of attack 6°, 2 kHz octave band, PPS 12/2 turbulence grid (not shown), including the three-dimensional integration sector for noise generated at the leading edge (blue cuboid).

3. Results and Discussion

3.1. Aerodynamic Performance

In this section, the aerodynamic performance of the airfoils modified with different leading-edge comb structures will be compared. To this end, Figure 7 shows the measured lift and drag forces as well as the lift-to-drag ratio of the modified airfoils, normalized with the values of the reference LS(1)0413 airfoil. Thereby, the given results are from measurements with the PPS 12/2 turbulence grid (but the trends obtained when using the PPS 14/4 turbulence grid were similar).

In general, most of the modifications appear to have only a small influence on the resulting aerodynamics over the complete range of flow speeds. The lift force at 6° angle of attack, shown in Figure 7a, is highest for the modified airfoils with straight teeth with a normalized spacing of 0.0095 (airfoils number 6 and 7 from Table 2) and straight teeth with a normalized spacing of 0.019 (airfoils number 3 and 4) and lowest for the modified airfoils with straight teeth and the largest spacing (airfoils 1 and 2). At 12° (Figure 7d), the highest lift is generated by the airfoil with curved teeth with a normalized length of 0.06 and a normalized spacing of 0.019. The LS(1)0413 airfoil that generates the lowest lift is again the one with straight teeth with a normalized length of 0.1 and a normalized spacing of 0.038. At the minimum, it generates about 83% of the value from the reference airfoil at an angle of attack of 6° and 93% at 12°.

The measured drag forces are shown in Figure 7b,e. The highest drag forces at an angle of attack of 6° are generated by the airfoil with straight teeth with a normalized length of 0.06 and a normalized spacing of 0.0095, with values that exceed those of the reference airfoil by up to 9%. At 12° angle of attack, the highest drag is generated by the airfoil with curved teeth with a normalized length of 0.06 and a spacing of 0.019. In this case, the measured drag forces exceed the values of the reference airfoil by up to 16%. One possible explanation for the very high drag forces measured for this airfoil is that, accidentally, an angle of attack slightly greater than 12° was adjusted. The lowest drag for the modified airfoils was measured for the airfoil with straight teeth with a normalized length of 0.01, which gives drag forces that are between 89% and 98% of the values obtained for the reference airfoil at 6° angle of attack and between 95% and 100% at 12°. Overall, the results show that some of the comb structures lead to an increase in drag, while others actually reduce drag.

The resulting lift-to-drag ratios, as probably the most important parameter to judge the aerodynamic performance of the different modifications, are shown in Figure 7c,f for angles of attack of 6° and 12°, respectively. It can be seen that basically all leading edges modified with combs that have curved teeth lead to a decrease in lift-to-drag-ratio, with maximum reductions around 11% to 13% for the airfoil with curved teeth with a normalized length of 0.06 and spacing of 0.019. Overall, the best performance can be observed for the airfoils modified with straight teeth of equal length with the medium spacing of 0.019 c_l (airfoils 3 and 4), yielding normalized lift-to-drag ratios between 95% and 104%. Good results, with normalized ratios between 95% and 100%, are also visible for the airfoils with teeth of equal length, but the largest spacing of 0.038 c_l (airfoils 1 and 2).
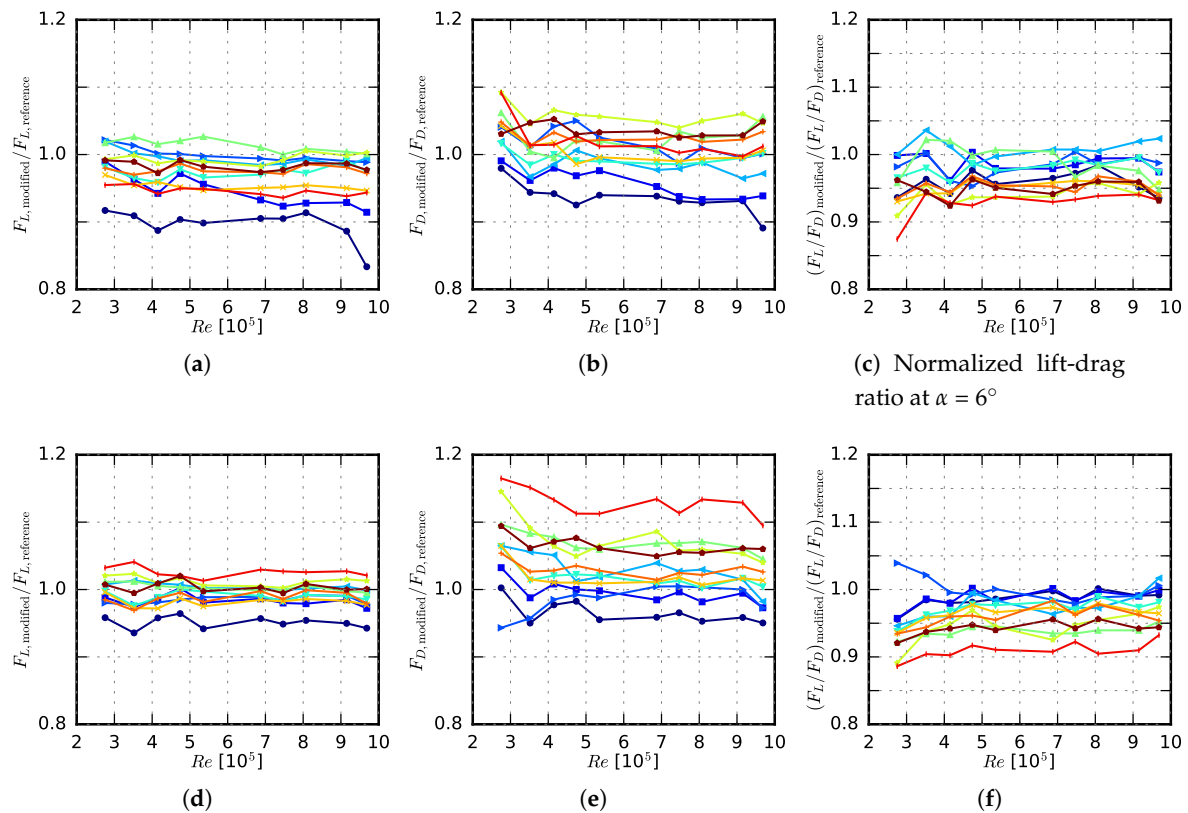

Figure 7. Aerodynamic forces of the airfoils with different leading edge comb structures, normalized with the corresponding values of the reference LS(1)0413 airfoil, PPS 12/2 turbulence grid (airfoil ● 1, ■ 2, ▶ 3, ◀ 4, ▼ 5, ▲ 6, ✦ 7, ✕ 8, + 9, ❙ 10, ⬠ 11), (**a**) normalized lift force at $\alpha = 6°$, (**b**) normalized drag force at $\alpha = 6°$, (**c**) normalized lift-drag ratio at $\alpha = 6°$, (**d**) normalized lift force at $\alpha = 12°$, (**e**) normalized drag force at $\alpha = 12°$, (**f**) normalized lift-drag ratio at $\alpha = 12°$.

This shows that, overall, the aerodynamic performance of the modified LS(1)0413 airfoils is not significantly lower than that of the reference airfoil. It is known that certain leading-edge protuberances, while giving a reduction in lift and drag at angles of attack below the stall angle, may actually lead to an improved aerodynamic performance in the post-stall regime [44]. This was also confirmed for an airfoil modified with serrations directly inspired by the leading edge comb of owls [45], where flow visualization tests showed that the serrations helped to delay stall. Although in the present study no measurements were performed at post-stall angles, such experiments should be part of future investigations.

3.2. Acoustic Performance

In this section, results will be presented for the measurements of the noise generated at the leading edge of the airfoils. As an example, Figure 8 shows sound pressure level spectra measured with two different turbulent inflow conditions, but a similar flow speed of approximately 40 m/s and an angle of attack of 6°. Results obtained with the turbulence grid PPS 12/2, which generates turbulence with an intensity of 4.6% and a streamwise integral length scale of 5.0 mm, are shown in Figure 8a. Figure 8b shows results obtained with the PPS 14/4 grid, which generates turbulence with a slightly increased intensity and length scale of 5.0% and 5.9 mm, respectively. Overall, the acoustic effect of the leading edge comb structures as a whole seems to be quite small. Basically, it can be seen that some of the modifications lead to a small noise reduction only, mainly at low and medium frequencies, while more or less all modifications lead to a noticeable noise increase at high frequencies approximately above 6.3 kHz. Some of the comb structures, however, generate a sound pressure level above that of the reference airfoil in the whole range of frequencies.
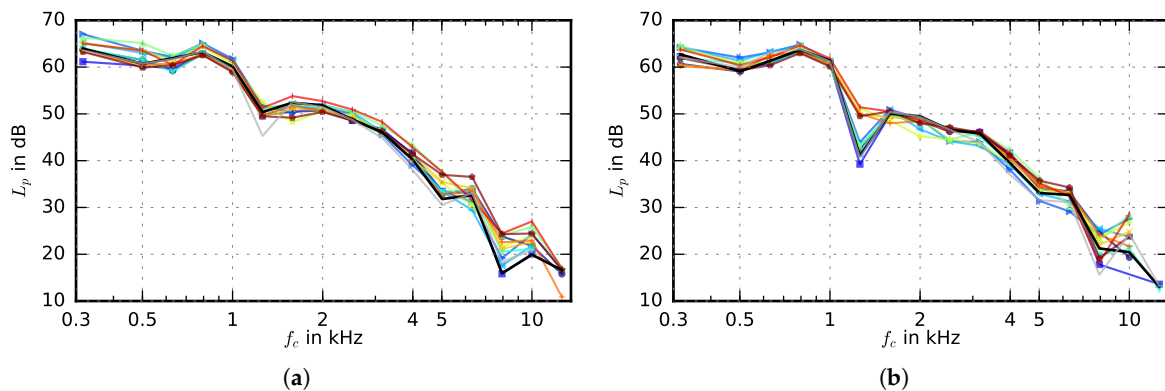

(**a**)   (**b**)

Figure 8. One third octave band sound pressure level spectra at $U \approx 40$ m/s and $\alpha = 6°$ (airfoil ● 1, ■ 2, ▶ 3, ◀ 4, ▼ 5, ▲ 6, ✦ 7, × 8, + 9, ❙ 10, ⬠ 11), (**a**) PPS 12/2 turbulence grid, $U = 40.5$ m/s, $Tu = 4.6\%$, $\Lambda = 5.0$ mm, (**b**) PPS 14/4 turbulence grid, $U = 38.7$ m/s, $Tu = 5.0\%$, $\Lambda = 5.8$ mm.

In order to obtain a more practically usable metric for the comparison of the acoustic performance of the different comb structures, the overall sound pressure level from the third octave bands with frequencies between 315 Hz and 10 kHz can be calculated as follows:

$$OSPL = 10 \cdot \log_{10} \left(\sum_{f_c=315 \text{ Hz}}^{10 \text{ kHz}} 10^{\frac{Lp}{10 \text{ dB}}} \right) \text{ dB}. \tag{2}$$

In Figure 9, the difference between the overall sound pressure level of the reference airfoil and that of the modified airfoils

$$\Delta OSPL = OSPL_{\text{reference}} - OSPL_{\text{modified}}, \tag{3}$$

is shown for both turbulence grids and all three angles of attack as a function of flow speed.

Basically, two groups of modifications can be clearly recognized: One group leads to an increase of the overall sound pressure level (corresponding to negative values of the overall sound pressure level difference shown in Figure 9), while the other has a positive acoustic effect and leads to a reduction of the overall sound pressure level. This is basically true for both turbulence grids and all angles of attack, although the results are more easily distinguishable for the cases with the PPS 12/2 turbulence grid (Figure 9a,c,e). Airfoils that lead to a noise increase are the ones with the numbers 3, 4, 6, 7 and 10 (see Table 2), which corresponds to combs with straight teeth of equal length and a medium spacing of 0.019 c_l (no. 3 and 4), combs with straight teeth with the small spacing of 0.0095 c_l (no. 6 and 7)

and combs with curved teeth with equal length and medium spacing (no. 10). The airfoils that show consistently good acoustic results are the ones modified with teeth that either have a large spacing of 0.038 c_l (no. 1, 2, 8, 9) or that have teeth of alternating length (no. 5 and 11). Since for the structures that feature teeth of alternating length the spacing between only the longer teeth corresponds to the same large spacing of 0.038 c_l, it can be concluded that a large spacing of the teeth seems to be most favorable regarding the overall noise reduction. When additionally taking into account the good aerodynamic results in terms of the lift-to-drag ratio for the two airfoils modified with combs with straight teeth and large spacing (no. 1 and 2), as presented in Section 3.1, it can be concluded that these modifications overall are the most beneficial. The use of these combs leads to a notable reduction of turbulence interaction noise with only negligible aerodynamic losses.
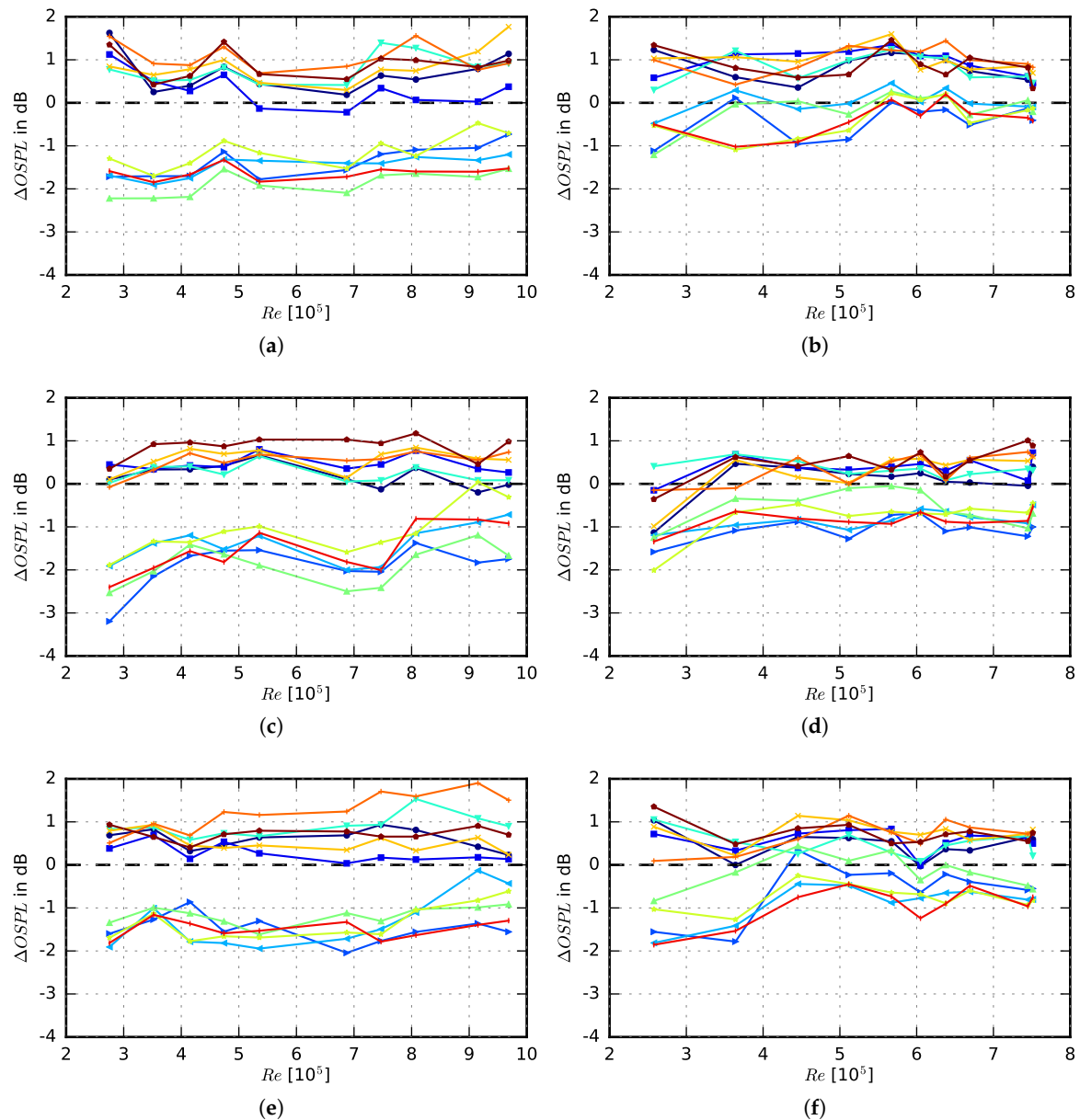

Figure 9. Difference of overall sound pressure level according to Equations (2) and (3) (airfoil ● 1, ■ 2, ▶ 3, ◀ 4, ▼ 5, ▲ 6, ✶ 7, × 8, + 9, | 10, ⬟ 11; positive values denote a noise reduction due to the modifications, negative values a noise increase), (**a**) PPS 12/2, $\alpha = 0°$, (**b**) PPS 14/4, $\alpha = 0°$, (**c**) PPS 12/2, $\alpha = 6°$, (**d**) PPS 14/4, $\alpha = 6°$, (**e**) PPS 12/2, $\alpha = 12°$, (**f**) PPS 14/4, $\alpha = 12°$.

In a second step, in order to be able to distinguish the effect of the different modifications more clearly, the sound pressure level differences between the noise generated by the baseline LS(1)-0413 airfoil and the noise generated by the modified airfoils,

$$\Delta L_p = L_{p,\text{reference}} - L_{p,\text{modified}}, \tag{4}$$

will be analyzed. The results are shown exemplarily in Figures 10–12 for the combs with teeth with a normalized length of $h/c_l = 0.06$, $h/c_l = 0.1$ and alternating length ($h/c_l = 0.06$ and 0.1), respectively, as a function of frequency and Reynolds number. Note that in each figure, the plots are ordered by the spacing of the teeth, from the largest ($s/c_l = 0.038$) to the smallest ($s/c_l = 0.0095$). The results were obtained with the PPS 12/2 turbulence grid at an angle of attack of 6°. Thereby, the measured third octave band sound pressure level data were interpolated using a two-dimensional Clough–Tocher scheme [46] in order to obtain a better resolution.

From these figures, regions can now be observed in more detail where the modifications lead to a reduction of leading-edge noise as opposed to regions where an increase in noise occurs. There are a few cases where it is obvious that the modifications do not lead to a leading-edge noise reduction at all (especially airfoils 4, 6 and 10, see Figures 10c,d and 11d, respectively). There are some other modifications for which the contour plots do not yield a clear trend, due to the fact that they contain both notable regions of noise increase, but also clearly distinguishable regions of noise reduction. This is true for the airfoils 3 (Figure 11c) and 7 (Figure 10e). For those two, however, the analysis of the overall sound pressure level difference (Figure 9) already showed that the comb structures lead to an increase in total noise. Apart from those cases, it is visible that reductions appear mainly at low and medium frequencies, from about 500 Hz to approximately 1 kHz at the lowest Reynolds number and 5 kHz at the maximum Reynolds number. The corresponding frequency range increases towards higher frequencies with increasing Reynolds number. At medium frequencies (starting at approximately 1.25 kHz at the lowest Reynolds number), a gradual increase in noise with frequency can be observed. However, when increasing the Reynolds number, the lower frequency limit of the region in which this increase in noise is found gradually shifts toward higher frequencies. Finally, at the highest Reynolds numbers, no noticeable increase of noise occurs at medium frequencies. At frequencies above approximately 6.3 kHz, it is difficult to draw conclusions about the emitted noise, since several, smaller regions of noise reduction and regions of noise increase are visible. It can be observed qualitatively, though, that generally airfoils with a large spacing between the teeth of the combs (airfoil 2, Figure 10a, airfoil 9, Figure 10b, airfoil 1, Figure 11a and airfoil 8, Figure 11b) as well as the two airfoils with teeth of alternating length (airfoil 5, Figure 12a and airfoil 11, Figure 12b) show the best overall acoustic performance.

The fact that many modifications lead to a noise reduction at low frequencies combined with a noise increase at high frequencies, which is evident in Figure 8 through Figure 12, allows for conclusions on the possible working principle of the leading edge combs. One hypothesis is that the comb structures break up the incoming turbulent eddies, effectively reducing their size until they are in the order of magnitude of the spacing between the teeth. Since the size of the turbulent eddies in the inflow is related to the frequency range of the emitted leading-edge noise (large eddies generate low-frequency noise, while small eddies generate high-frequency noise, see for example [47]), this break-up would lead to the observed frequency shift (of course, this breaking of the turbulent eddies can also lead to a generation of noise). Another possible reason for the noticeably increased noise at high frequencies observed in the present study is that the combs themselves are also a source of noise, like basically any sort of protrusion or surface roughness. The second hypothesis for the aeroacoustic effect of the combs is that they shift the turbulent eddies away from the airfoil surface, thus reducing the pressure fluctuations acting on the airfoil similar to canopies [48] or finlets [49] used for the reduction of trailing edge noise and roughness noise.
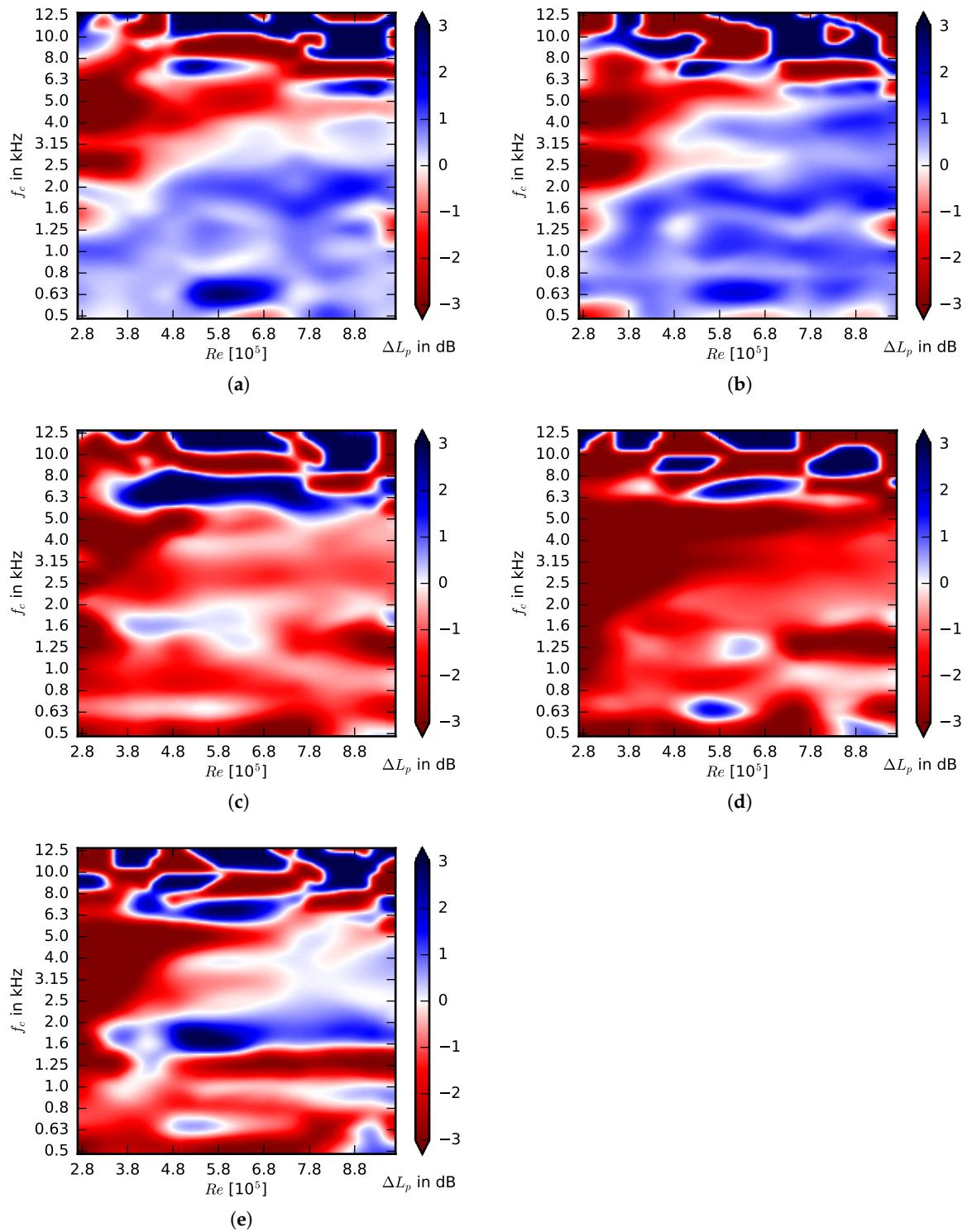
Figure 10. Leading edge sound pressure level difference ΔL_p according to Equation (4) for the airfoils with teeth of $h/c_l = 0.06$, angle of attack 6°, PPS 12/2 turbulence grid (positive values denote a noise reduction due to the modifications, negative values a noise increase), (**a**) airfoil 2, $h/c_l = 0.06$, $s/c_l = 0.038$, straight, (**b**) airfoil 9, $h/c_l = 0.06$, $s/c_l = 0.038$, curved, (**c**) airfoil 4, $h/c_l = 0.06$, $s/c_l = 0.019$, straight, (**d**) airfoil 10, $h/c_l = 0.06$, $s/c_l = 0.019$, curved, (**e**) airfoil 7, $h/c_l = 0.06$, $s/c_l = 0.0095$, straight.
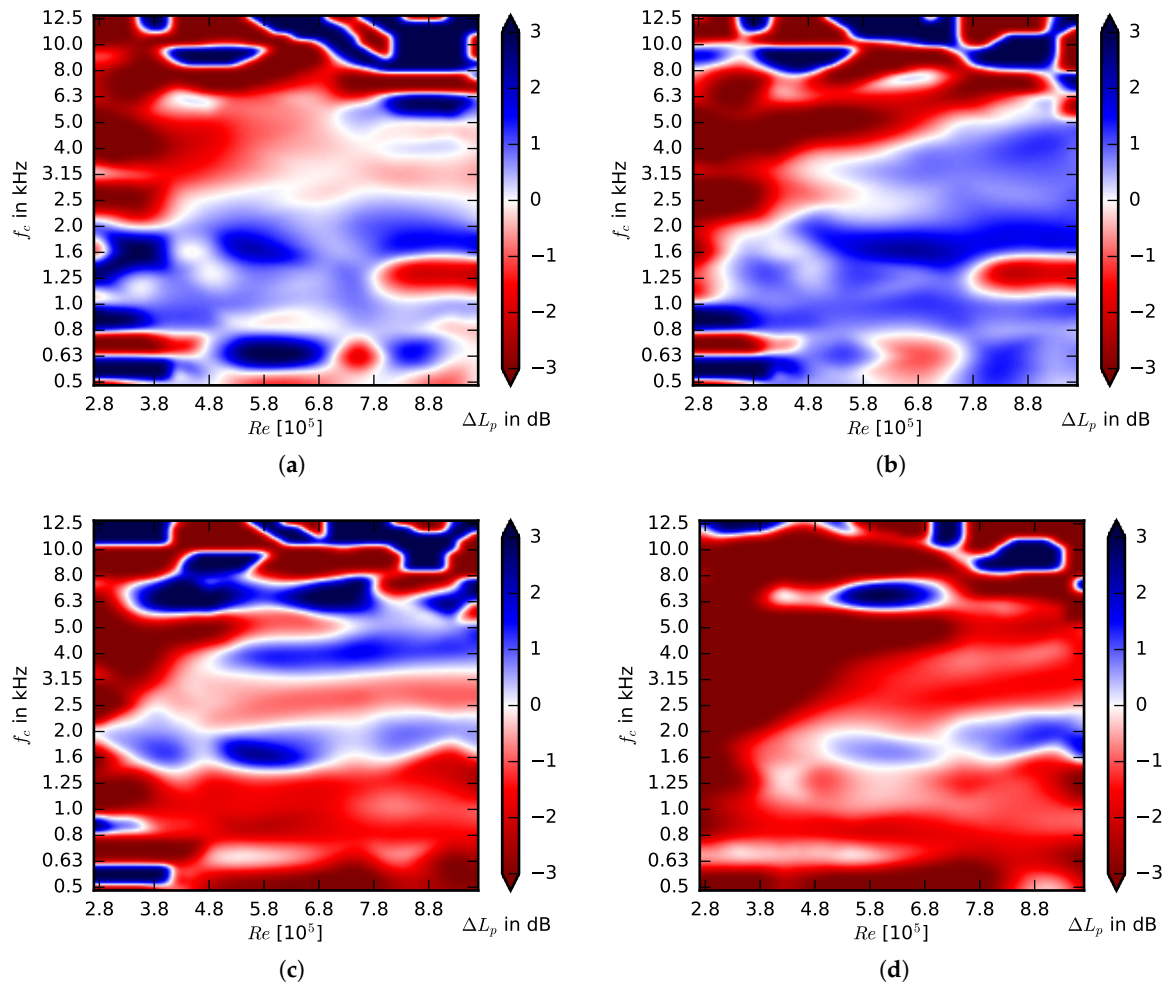
Figure 11. Leading edge sound pressure level difference ΔL_p according to Equation (4) for the airfoils with teeth of $h/c_l = 0.1$, angle of attack 6°, PPS 12/2 turbulence grid (positive values denote a noise reduction due to the modifications, negative values a noise increase), (**a**) airfoil 1, $h/c_l = 0.1$, $s/c_l = 0.038$, straight, (**b**) airfoil 8, $h/c_l = 0.1$, $s/c_l = 0.038$, curved, (**c**) airfoil 3, $h/c_l = 0.1$, $s/c_l = 0.019$, straight, (**d**) airfoil 6, $h/c_l = 0.1$, $s/c_l = 0.0095$, straight.

Thus, a very important design parameter seems to be the ratio of teeth spacing to the integral length scale, s/Λ_x (actually, the integral length scale in the spanwise direction, Λ_y, would be more fitting, but for isotropic turbulence the integral length scales are proportional). In general, it seems that a somewhat larger spacing of the teeth is beneficial, since overall good results at low frequencies were obtained for the combs with a spacing of 0.038 c_l between the single teeth (airfoils 1, 2, 8 and 9). For those, the spacing is 7.6 mm, which is slightly larger than the integral length scale of the turbulence generated by the grids (5 to 6 mm). Combs with teeth that have the smallest normalized spacing of 0.0095 c_l (airfoils 6 and 7) as well as combs with teeth of equal length, but medium spacing of 0.019 c_l (airfoils 3, 4 and 10) performed rather poorly. This spacing corresponds to values of only 1.9 mm and 3.8 mm, respectively, which is smaller than the integral length scale of the incoming turbulence. Thus, a spacing in the order of (or slightly larger than) the size of the turbulent eddies is favorable. This is very interesting since it is known that for leading-edge serrations a small serration wavelength results in a better performance than a large serration wavelength (see for example [7]). However, it is important to note that the spacing used in the present study is much smaller compared to typical serration wavelengths. Additionally, of the airfoils with the large spacing between the teeth, the ones with shorter teeth with a length of 0.06 c_l slightly outperform the airfoils having teeth with the same spacing, but a larger normalized length of 0.01. In conclusion, the present results imply that the combs

with a small spacing between the teeth rather break up the eddies, thus not leading to an overall noise reduction, while the combs with larger spacing between the teeth have a positive effect on the noise reduction. It is likely that they filter the incoming turbulent eddies, thereby causing a decorrelation of spanwise turbulent structures while also slightly shifting the eddies away from the airfoil surface.
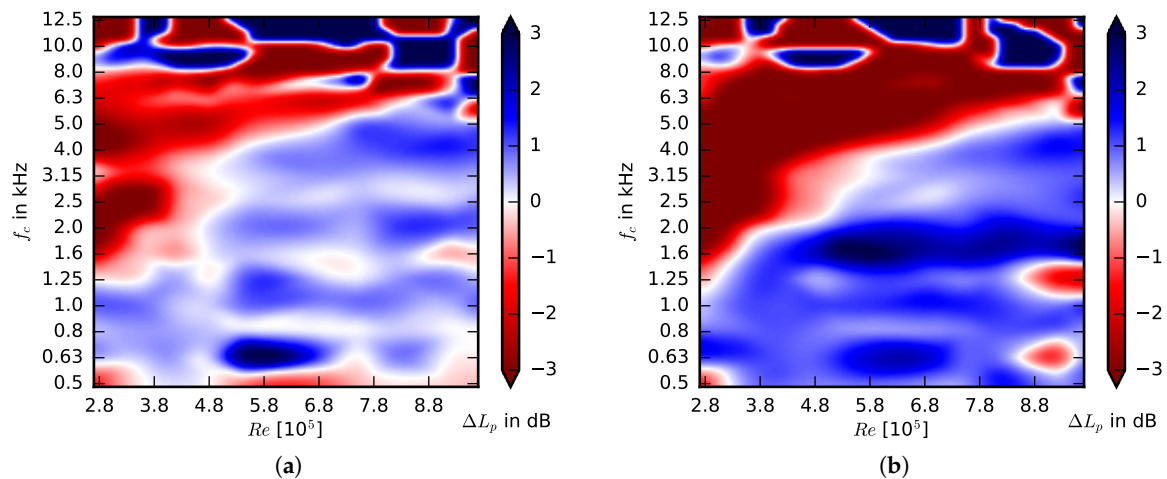

Figure 12. Leading edge sound pressure level difference ΔL_p according to Equation (4) for the airfoils with teeth of alternating length, angle of attack 6°, PPS 12/2 turbulence grid (positive values denote a noise reduction due to the modifications, negative values a noise increase), (**a**) airfoil 5, h/c_l = 0.06, 0.1, s/c_l = 0.019, straight, (**b**) airfoil 11, h/c_l = 0.06, 0.1, s/c_l = 0.019, curved.

Another conclusion that can be drawn from the present results (especially Figure 10 through Figure 12) is that the increase in noise reduction with increasing flow speed does not seem to be strictly limited to the range of flow speeds used in the present study. This means that for real wind turbine blades, which usually operate at even higher chord-based Reynolds numbers (Commercial wind turbines typically operate at Reynolds numbers in the order of $1\cdot10^6$ [50], based on the flow conditions at the blade tip.), the low-frequency noise-reducing effect of the examined comb structures may be even more significant.

4. Summary

An experimental study was performed to explore the effect of comb-like extensions at the leading edge of airfoils on the generation of turbulence interaction noise. The study took place in a small aeroacoustic wind tunnel, where the required turbulent inflow was generated by two different perforated plates. The airfoils of the type LS(1)-0413 had leading edges that were modified with steel pins, thus creating a comb-like structure. The length and spacing of these pins, which were either straight or slightly curved in an upward manner, was varied.

The results from the aerodynamic measurements showed that, overall, the comb structures do not change the aerodynamic performance significantly. Good results in terms of the lift-to-drag ratio can be obtained for the airfoils modified with combs consisting of straight teeth with medium (s/c_l = 0.019, normalized with airfoil chord length) and large spacing (s/c_l = 0.038). The results from the acoustic measurements showed that, overall, the influence of the comb structures is small. A noise reduction was observed at low frequencies below approximately 1.6 kHz, while at the same time more noise is generated at high frequencies. This observation implies the hypothesis that the function of the combs, especially those with a spacing between the teeth that are smaller than the size of the incoming turbulent structures, is to break up the incoming turbulent eddies, thereby reducing their size. This leads to a shift in the noise generated at the leading edge from lower to higher frequencies, but not necessarily to a reduction of the overall sound pressure level. The effect of combs with teeth that have a spacing in the order of or slightly larger than the size of the turbulent eddies is most

probably a filtering and a slight shift of the eddies further away from the airfoil surface, thus reducing the pressure fluctuations on the leading edge, plus a potential spanwise decorrelation of the turbulent structures. In general, the modifications that performed best in terms of the overall noise reduction and aerodynamic performance are combs with straight teeth with a large spacing.

It was found that the frequency range of the sound pressure level difference that can be obtained through the combs, compared to an airfoil with an unmodified leading-edge, increases with Reynolds number. The fact that this noise reduction seems not to be limited to the range of moderate Reynolds numbers of this study is especially promising when it is considered that wind turbines usually operate in a range of Reynolds numbers towards the maximum of the current study and above.

Abbreviations

The following abbreviations are used in this manuscript:

PPS   Perforated Plate with Square holes

References

1. Soderman, P.T. *Leading Edge Serrations Which Reduce the Noise of Low-Speed Rotors*; Technical Report, NASA Technical Note D-7371; National Aeronautics and Space Administration: Washington, DC, USA, 1973.
2. Hersh, A.S.; Soderman, P.T.; Hayden, R.E. Investigation of acoustic effects of leading-edge serrations on airfoils. *J. Aircr.* **1974**, *11*, 197–202. [CrossRef]
3. Gruber, M.; Joseph, P.; Polacsek, C.; Chong, T.P. Noise reduction using combined trailing edge and leading edge serrations in a tandem airfoil experiment. In Proceedings of the 18th AIAA/CEAS Aeroacoustics Conference, AIAA Paper 2012-2134, Colorado Springs, CO, USA, 4–6 June 2012.
4. Roger, M.; Schram, C.; De Santana, L. Reduction of airfoil turbulence-impingement noise by means of leading-edge serrations and/or porous materials. In Proceedings of the 19th AIAA/CEAS Aeroacoustics Conference, AIAA Paper 2013-2108, Berlin, Germany, 27–29 May 2013; pp. 27–29.
5. Liu, X.; Azarpeyvand, M.; Theunissen, R. Aerodynamic and Aeroacoustic Performance of Serrated Airfoils. In Proceedings of the 21st AIAA/CEAS Aeroacoustics Conference, AIAA Paper 2015-2201, Dallas, TX, USA, 22–26 June 2015.
6. Narayanan, S.; Chaitanya, P.; Haeri, S.; Joseph, P.; Kim, J.W.; Polacsek, C. Airfoil noise reductions through leading edge serrations. *Phys. Fluids* **2015**, *27*, 025109. [CrossRef]
7. Juknevicius, A.; Chong, T.P. On the leading edge noise and aerodynamics of thin aerofoil subjected to the straight and curved serrations. *J. Sound Vib.* **2018**, *425*, 324–343. [CrossRef]
8. Hansen, K.L.; Kelso, R.M.; Doolan, C.J. Reduction of flow induced tonal noise through leading edge tubercle modifications. In Proceedings of the 16th AIAA/CEAS Aeroacoustics Conference, AIAA Paper 2010-3700, Stockholm, Sweden, 7–9 June 2010; Volume 3700.
9. Polacsek, C.; Reboul, G.; Clair, V.; Le Garrec, T.; Deniau, H. Turbulence-airfoil interaction noise reduction using wavy leading edge: An experimental and numerical study. In Proceedings of the 40th International Congress and Exposition on Noise Control Engineering (INTER-NOISE), Osaka, Japan, 4–7 September 2011.
10. Clair, V.; Polacsek, C.; Le Garrec, T.; Reboul, G.; Gruber, M.; Joseph, P. Experimental and numerical investigation of turbulence-airfoil noise reduction using wavy edges. *AIAA J.* **2013**, *51*, 2695–2713. [CrossRef]

11. Chong, T.P.; Vathylakis, A.; McEwen, A.; Kemsley, F.; Muhammad, C.; Siddiqi, S. Aeroacoustic and aerodynamic performances of an aerofoil subjected to sinusoidal leading edges. In Proceedings of the 21st AIAA/CEAS Aeroacoustics Conference, AIAA Paper 2015-2200, Dallas, TX, USA, 22–26 June 2015.

12. Chaitanya, P.; Joseph, P.; Narayanan, S.; Vanderwel, C.; Turner, J.; Kim, J.W.; Ganapathisubramani, B. Performance and mechanism of sinusoidal leading edge serrations for the reduction of turbulence–aerofoil interaction noise. *J. Fluid Mech.* **2017**, *818*, 435–464. [CrossRef]

13. Chaitanya, P.; Joseph, P.; Narayanan, S.; Kim, J. Aerofoil broadband noise reductions through double-wavelength leading-edge serrations: A new control concept. *J. Fluid Mech.* **2018**, *855*, 131–151. [CrossRef]

14. Biedermann, T.M.; Chong, T.P.; Kameier, F.; Paschereit, C.O. Statistical–Empirical Modeling of Airfoil Noise Subjected to Leading-Edge Serrations. *AIAA J.* **2017**, *55*, 3128–3142. [CrossRef]

15. Biedermann, T.M.; Czeckay, P.; Geyer, T.F.; Kameier, F.; Paschereit, C.O. Effect of Inflow Conditions on the Noise Reduction Through Leading Edge Serrations. *AIAA J.* **2019**, *57*, 4104–4109. [CrossRef]

16. Chaitanya, P.; Joseph, P. Slitted leading edge profiles for the reduction of turbulence-aerofoil interaction noise. *J. Acoust. Soc. Am.* **2018**, *143*, 3494–3504. [CrossRef]

17. Geyer, T.F.; Sarradj, E.; Giesler, J.; Hobracht, M. Experimental assessment of the noise generated at the leading edge of porous airfoils using microphone array techniques. In Proceedings of the 17th AIAA/CEAS Aeroacoustics Conference, AIAA Paper 2011-2713, Portland, OR, USA, 5–8 June 2011.

18. Geyer, T.F.; Lucius, A.; Schrödter, M.; Schneider, M.; Sarradj, E. Reduction of Turbulence Interaction Noise Through Airfoils With Perforated Leading Edges. *Acta Acust. United Acust.* **2019**, *105*, 109–122. [CrossRef]

19. Lau, A.S.H.; Haeri, S.; Kim, J.W. The effect of wavy leading edges on aerofoil–gust interaction noise. *J. Sound Vib.* **2013**, *332*, 6234–6253. [CrossRef]

20. Chen, W.; Qiao, W.; Wang, L.; Tong, F.; Wang, X. Rod-Airfoil Interaction Noise Reduction Using Leading Edge Serrations. In Proceedings of the 21st AIAA/CEAS Aeroacoustics Conference, AIAA Paper 2015-3264, Dallas, TX, USA, 22–26 June 2015.

21. Kim, J.W.; Haeri, S.; Joseph, P.F. On the reduction of aerofoil–turbulence interaction noise associated with wavy leading edges. *J. Fluid Mech.* **2016**, *792*, 526–552. [CrossRef]

22. Mathews, J.; Peake, N. Noise generation by turbulence interacting with an aerofoil with a serrated leading edge. In Proceedings of the 21st AIAA/CEAS Aeroacoustics Conference, AIAA Paper 2015-2204, Dallas, TX, USA, 22–26 June 2015.

23. Zhang, M.; Frendi, A. Effect of airfoil leading edge waviness on flow structures and noise. *Int. J. Numer. Methods Heat Fluid Flow* **2016**, *26*, 1821–1842. [CrossRef]

24. Lyu, B.; Azarpeyvand, M. On the noise prediction for serrated leading edges. *J. Fluid Mech.* **2017**, *826*, 205–234. [CrossRef]

25. Ayton, L.J. Analytic solution for aerodynamic noise generated by plates with spanwise-varying trailing edges. *J. Fluid Mech.* **2018**, *849*, 448–466. [CrossRef]

26. Tong, F.; Qiao, W.; Xu, K.; Wang, L.; Chen, W.; Wang, X. On the study of wavy leading-edge vanes to achieve low fan interaction noise. *J. Sound Vib.* **2018**, *419*, 200–226. [CrossRef]

27. Lyu, B.; Ayton, L.J.; Chaitanya, P. On the acoustic optimality of leading-edge serration profiles. *J. Sound Vib.* **2019**, *462*, 114923. [CrossRef]

28. Lee, S. Reduction of Blade-Vortex Interaction Noise through Porous Leading Edge. *AIAA J.* **1994**, *32*, 480–488. [CrossRef]

29. Tinetti, A.; Kelly, J.; Thomas, R.; Bauer, S. Reduction of Wake-Stator Interaction Noise Using Passive Porosity. In Proceedings of the 40th AIAA Aerospace Sciences Meeting and Exhibit, AIAA Paper 2002-1036, Reno, NV, USA, 14–17 January 2002.

30. Wasala, S.H.; Norris, S.E.; Cater, J.E. Wind turbine noise reduction by blade geometry modification. In Proceedings of the 22nd International Congress on Sound and Vibration, Florence, Italy, 12–16 July 2015.

31. Graham, R.R. The silent flight of owls. *J. R. Aeronaut. Soc.* **1934**, *286*, 837–843. [CrossRef]

32. Geyer, T.F.; Claus, V.T.; Hall, P.M.; Sarradj, E. Silent owl flight: The effect of the leading edge comb. *Int. J. Aeroacoust.* **2017**, *16*, 115–134. [CrossRef]

33. Hertel, H. *Struktur, Form, Bewegung*; Otto Krauskopf-Verlag: Mainz, Germany, 1963; [translated version: Milton S. Katz (ed.), Structure, Form, Movement. Reinhold, New York (1966)].

34. Lilley, G. A study of the silent flight of the owl. In Proceedings of the 4th AIAA/CEAS Aeroacoustics Conference, AIAA Paper 1998-2340, Toulouse, France, 2–4 June 1998.

35. Sarradj, E.; Fritzsche, C.; Geyer, T.F.; Giesler, J. Acoustic and Aerodynamic Design and Characterization of a Small-Scale Aeroacoustic Wind Tunnel. *Appl. Acoust.* **2009**, *70*, 1073–1080. [CrossRef]

36. Roach, P.W. The Generation of Nearly Isotropic Turbulence by Means of Grids. *Int. J. Heat Fluid Flow* **1987**, *8*, 82–92. [CrossRef]

37. Kurian, T.; Fransson, J.H.M. Grid-generated turbulence revisited. *Fluid Dyn. Res.* **2009**, *41*, 021403. [CrossRef]

38. Geyer, T.F.; Hobracht, M.; Sarradj, E. Noise generated by a leading edge in anisotropic turbulence. In *INTER-NOISE and NOISE-CON Congress and Conference Proceedings*; Institute of Noise Control Engineering: Hamburg, Germany, 2016; Volume 253, pp. 1176–1187.

39. Hinze, J.O. *Turbulence*, 2nd ed.; McGraw-Hill: New York, NY, USA 1975.

40. Brooks, T.F.; Marcolini, M.A.; Pope, D.S. Airfoil Trailing Edge Flow Measurements and Comparison with Theorie incorporating Open Wind Tunnel Corrections. In Proceedings of the 9th AIAA/NASA Aeroacoustics Conference, AIAA Paper 84-2266, Williamsburg, VA, USA, 15–17 October 1984.

41. Sarradj, E. A fast ray casting method for sound refraction at shear layers. *Int. J. Aeroacoust.* **2017**, *16*, 65–77. [CrossRef]

42. Sijtsma, P. CLEAN based on Spatial Source Coherence. *Int. J. Aeroacoust.* **2007**, *6*, 357–374. [CrossRef]

43. Sarradj, E. Three-dimensional acoustic source mapping with different beamforming steering vector formulations. *Adv. Acoust. Vib.* **2012**, *2012*, 292695. [CrossRef]

44. Johari, H.; Henoch, C.; Custodio, D.; Levshin, A. Effects of Leading-Edge Protuberances on Airfoil Performance. *AIAA J.* **2007**, *45*, 2634–2642. [CrossRef]

45. Ito, S. Aerodynamic Influence of Leading-Edge Serrations on an Airfoil in a Low Reynolds Number. *J. Biomech. Sci. Eng.* **2009**, *4*, 117–123. [CrossRef]

46. Alfeld, P. A trivariate Clough–Tocher scheme for tetrahedral data. *Comput. Aided Geom. Des.* **1984**, *1*, 169–181. [CrossRef]

47. Wagner, S.; Bareiss, R.; Guidati, G. *Wind Turbine Noise*; Springer Science & Business Media: Berlin/Heidelberg, Germany, 2012.

48. Clark, I.A.; Daly, C.A.; Devenport, W.; Alexander, W.N.; Peake, N.; Jaworski, J.W.; Glegg, S. Bio-inspired canopies for the reduction of roughness noise. *J. Sound Vib.* **2016**, *385*, 33–54. [CrossRef]

49. Clark, I.A.; Alexander, W.N.; Devenport, W.; Glegg, S.; Jaworski, J.W.; Daly, C.; Peake, N. Bioinspired trailing-edge noise control. *AIAA J.* **2017**, *55*, 740–754. [CrossRef]

50. McTavish, S.; Feszty, D.; Nitzsche, F. Evaluating Reynolds number effects in small-scale wind turbine experiments. *J. Wind Eng. Ind. Aerodyn.* **2013**, *120*, 81–90. [CrossRef]